FACTA UNIVERSITATIS
Series: **Electronics and Energetics** Vol. 38, Nº 4, December 2025, pp. 715 - 736
https://doi.org/10.2298/FUEE2504715G

Original scientific paper

REAL-TIME MONITORING OF STRUCTURAL VIBRATIONS USING ADVANCED FBG SENSOR NETWORKS

Mouna Garai, Maha Sliti, Noureddine Boudriga

University of Carthage, Higher School of Communication of Tunis (SUP'COM), LR11TIC04, Communication Networks and Security Research Lab. & LR11TIC02, Green and Smart Communication Systems Research Lab, Tunisia

ORCID iDs:	Mouna Garai	https://orcid.org/0000-0001-8224-5666
	Maha Sliti	https://orcid.org/0000-0002-8296-6284
	Noureddine Boudriga	https://orcid.org/0000-0002-5720-0164

Abstract. *This paper explores the use of Fiber Bragg Grating (FBG) sensors in structural health monitoring (SHM) systems, emphasizing their role in sustainable urban development. The proposed system integrates a network of FBG sensors to enable real-time monitoring of structural vibrations, ensuring early detection of potential failures. Compared to conventional monitoring systems, our approach provides improved accuracy, enhanced durability, and resistance to electromagnetic interference. Additionally, the system allows for precise measurements of fiber deformation and sensor displacement in response to external conditions such as strain and environmental factors. A comparative analysis, based on literature benchmarks, demonstrates that the proposed FBG-based approach offers superior sensitivity, higher scalability, and more efficient data acquisition. Key performance metrics such as response time, strain sensitivity, and measurement precision highlight its advantages over traditional SHM techniques. These features make FBG sensors an optimal solution for monitoring infrastructure such as bridges, buildings, and railway networks, thereby contributing to the sustainability and longevity of urban structures.*

Key words: *Fiber Bragg Grating, vibration detection, optical sensors, structure health monitoring*

1. INTRODUCTION

Civil engineering infrastructures such as buildings and bridges continue to operate despite degradation and associated dangers. Structural health monitoring (SHM) systems are critical for both economic reasons and safety assurance. These systems consist of a network of sensor arrays that are designed to detect and forecast structural damage. The aim of early damage detection is to reduce both repair costs and time frames. The system

Received January 12, 2025; revised February 18, 2025 and February 27, 2025; accepted February 27, 2025
Corresponding author: Maha Sliti
University of Carthage, Higher School of Communication of Tunis (SUP'COM)
E-mail: slitimaha@gmail.com

effectively mitigates the risk of unforeseen failures by collecting real-time data on the structure's vibrations.

Conventional instruments such as strain gauges and accelerometers are prone to issues such as leakage, illumination, and decay, which can result in inaccurate outcomes [1, 2, 3]. Optical fiber-sensing networks have attracted considerable attention compared to conventional sensors because of their resistance to electromagnetic interference. Fiber Bragg Grating (FBG) is a prominent optical fiber sensing technology (OFFT), recognized for its compact dimensions, remote sensing abilities, and durability in challenging environmental conditions [4, 5]. Furthermore, FBG sensors are capable of detecting physical parameters, including strain and temperature [6]. In addition, contemporary network designs are being developed with an emphasis on fiber and 5G technology. Integrating structural health monitoring systems with fiber optic networks is achievable through the installation of optical sensors for the monitoring of public buildings, highways, and bridges [7, 8].

This research extends our work in [9, 10]. This study introduces a comprehensive vibration monitoring framework utilizing the established FBG sensor network. The proposed SHM architecture can be parameterized after evaluating the application domains and the monitored structure. The suggested vibration monitoring architecture may estimate many metrics, including fiber deformation, FBG sensor displacement, and vibration. The computed vibration values can be decreased by an alert triggered by the collected measurements. This study analyzes the bridge scenario to assess the effectiveness of the proposed vibration monitoring framework. FBG sensors placed on bridges identify structural damage resulting from earthquakes, wind, vehicular loads, and other factors.

The current work includes the following contributions :

- A comprehensive vibration monitoring strategy is proposed that encompasses the physical network architecture, the system configuration, and the vibration estimation method. The proposed methodology is applicable to various vibration monitoring applications and systems. This is illustrated by a case study of the Vincent-Thomas Bridge (VTB).
- We suggest a fiber discretization approach to approximate the strain-induced deformation of the latter, regardless of the fiber length or curves in the monitored structure. This is accomplished by using two types of FBG sensors. The first type of FBG sensor is deployed at strategic points throughout the monitored structure. The second type of FBG sensor (support sensors) is inserted between two FBG sensors to improve the fiber deformation approximation under strain.
- We outline the mathematical methods employed to determine the displacement and average vibration at a critical point monitored by a fiber Bragg grating sensor. The proposed methodology for vibration analysis utilizes the physical properties of the FBG sensor, which vary in response to applied strain. The strain causes a change in the wavelength of the reflected signal. This transition enables the assessment of fiber deformation, the displacement of the FBG sensor, and the average vibration.

The organization of the paper is as follows. Section 2 discusses the related literature. Section 3 describes the principle working principle of FBG sensors. Section 4 outlines the fundamental components of the proposed FBG vibration monitoring architecture. Section 5 outlines the mathematical elements required to measure vibrations at a critical location monitored by an FBG sensor. Section 6 presents a case study on the implementation of a vibration monitoring strategy used on the Vincent-Thomas Bridge. Section 7 examines the efficacy and scalability of the proposed vibration monitoring system. Section 8

presents the simulation results derived from real displacement signals obtained from the Vincent Thomas Bridge during an earthquake. Section 9 concludes the paper.

2. Literature Review

Structural Health Monitoring (SHM) is essential for ensuring the safety and longevity of civil infrastructure, and various sensing technologies have been explored for this purpose. Among them, Fiber Bragg Grating (FBG) sensors have gained significant attention due to their unique advantages over conventional sensor types such as electrical strain gauges, piezoelectric sensors, accelerometers, and wireless sensor networks (WSNs).

Electrical strain gauges are widely used in SHM due to their simplicity and cost-effectiveness. They measure strain based on changes in electrical resistance. However, their performance is limited by electromagnetic interference (EMI), temperature sensitivity, and signal degradation over long distances. In contrast, FBG sensors, which operate on optical principles, are immune to EMI, exhibit higher durability, and can provide multiplexed sensing capabilities over a single optical fiber [11].

Piezoelectric sensors are commonly used for vibration and acoustic emission monitoring in SHM. While they offer high sensitivity and fast response times, their performance is influenced by environmental factors such as humidity and temperature variations. Additionally, they require electrical wiring and signal conditioning, making large-scale deployment challenging. FBG sensors, on the other hand, provide accurate strain and temperature measurements, are resistant to harsh environmental conditions, and do not require electrical power at the sensing location, reducing the risk of electrical failure [12].

Accelerometers, including MEMS-based accelerometers, are widely used in SHM for detecting structural vibrations and dynamic responses. While MEMS accelerometers offer advantages such as miniaturization and low power consumption, they can suffer from drift and require frequent calibration to maintain accuracy. Additionally, their performance is affected by temperature variations and long-term stability issues. In comparison, FBG-based accelerometers offer high precision, immunity to electromagnetic interference, and superior long-term stability, making them more reliable for continuous monitoring applications [13].

WSNs have been increasingly adopted in SHM due to their ease of deployment and ability to provide real-time data wirelessly. However, WSNs face limitations in terms of power consumption, data transmission reliability, and susceptibility to environmental noise. Moreover, the need for periodic battery replacement increases maintenance costs. FBG sensors, being passive optical devices, do not require an external power source at the sensing points and can be embedded into structures for long-term monitoring with minimal maintenance [13]. Table 1 summarizes the key advantages of FBG sensors compared to other SHM technologies:

Table 1 Advantages of FBG sensors compared to other SHM technologies

Sensor Type	EMI Resistance	Multiplexing Capability	Environmental Stability	Power Requirement	Maintenance Need
FBG Sensors	High	High	High	Low (Passive)	Low
Electrical Strain Gauges	Low	Low	Moderate	High	High
Piezoelectric Sensors	Low	Low	Moderate	High	Moderate
MEMS Accelerometers	Low	Moderate	Moderate	Moderate	Moderate

Based on the comparison, FBG sensors exhibit several advantages, including immunity to electromagnetic interference, high multiplexing capability, robustness in harsh environments, and minimal power requirements. These features make FBG sensors an ideal choice for long-term, reliable SHM applications, particularly in large-scale civil infrastructure projects. While other sensor technologies continue to play a role in SHM, FBG sensors are increasingly being integrated into smart monitoring systems due to their superior performance and long-term cost-effectiveness.

FBG sensors have facilitated notable progress in structural health monitoring within the aerospace and mechanical sectors by providing accurate real-time monitoring in dynamic environments. Zhou et al. [14] conducted a review of aviation applications, emphasizing their ability to monitor structural stress and deformation during flight. This study emphasized the importance of FBG sensors in ensuring safety and performance in metallic aviation structures. Goossens et al. [15] integrated FBG sensors into UAV composite materials to assess the distribution of strain during flight, confirming their effectiveness for lightweight and sensitive structures. Ho et al. [16] utilized FBG sensors within a cyber-physical system to monitor robotic linear systems, demonstrating their versatility in mechanical applications.

Marine structures have also benefited from innovations in Bragg fiber gratings. Gao et al. [17] developed a shape-sensing system specifically for cylindrical marine structures, facilitating real-time monitoring of deformation in challenging marine environments. Their research established the reliability of FBG technology for maritime structural health monitoring, addressing issues such as water pressure and dynamic loads.

Advanced monitoring frameworks that use machine learning and digital twins The incorporation of advanced technologies, including machine learning and digital twins, has significantly improved the functionalities of FBG sensors. Saha et al. [18] introduced a multi-array FBG system enhanced by machine learning, capable of differentiating between strain and temperature variations. This innovation facilitated enhanced monitoring accuracy in dynamic environments. Similarly, Lei et al. [19] investigated a twin-driven digital structural health monitoring framework that integrates Bragg fiber grating sensors with virtual modeling to forecast structural performance in diverse scenarios.

Comparative studies have demonstrated the advantages of FBG sensors in relation to traditional systems. Ibrar Jahan et al. [20] conducted a comparison between FBG technology and conventional strain gauge systems, concluding that FBG sensors provide superior accuracy, enhanced resistance to environmental factors, and increased versatility for various applications.

FBG sensors have been used in specialized applications. Wu et al. [21] employed ultrasonic structural health monitoring using FBG sensors, effectively demonstrating precise anomaly detection under high frequency stress conditions. Soman et al. [22] optimized the placement of FBGs through evolutionary strategies for ultrasonic monitoring, specifically targeting high-demand industrial and maritime applications.

Recent studies have concentrated on novel sensor designs, interdisciplinary integration, and new applications for FBG technology. Wang et al. [23] presented a comprehensive review of fiber Bragg grating applications, highlighting their versatility and scalability. Braunfelds et al. [24] investigated the integration of FBGs in road surfaces for the purpose of real-time load monitoring, thus facilitating the development of intelligent road systems. Jinghong et al. [25] examined the application of FBG in tunnels, focusing on safety issues within

high-speed railway systems. Table 2 presents a comparative overview of FBG Sensor Applications in SHM.

Table 2 Comparative overview of FBG sensor applications in SHM

Application Field	Specific Use Case	Key Advantages	References
Civil Engineering	Monitoring bridge stability post-earthquake	Real-time data collection, long sensing range, non-invasive monitoring	[10,13,14,26,27]
Mechanical Engineering	Train tracking and trespass detection	High sensitivity to strain and vibration, compact and robust design	[18,28]
Aerospace Engineering	Monitoring wing deformation and UAV damage detection	Compatibility with harsh environments, lightweight, and non-invasive	[15,17,29]
Subterranean Structures	Fracture propagation analysis in underground tunnels	High accuracy in stress detection, durability under extreme conditions	[25,30]
Transportation Tunnels	Detecting surface incursions and structural anomalies	Efficient vibration signal analysis using advanced signal processing techniques	[21,31]
Composite Materials	Monitoring the structural health of aerospace-grade composites	Durable under in-flight conditions, resistant to environmental stress	[29,32]
Marine Structures	Shape sensing for cylindrical marine structures	Real-time monitoring of deformation under harsh marine conditions	[17]
Road Pavements	Monitoring road pavement degradation and load-induced stress	Embedded in road surfaces for continuous real-time data collection	[24]
High-Speed Railways	Monitoring of large-section tunnels and railway track conditions	High precision and real-time feedback, effective in dynamic environments	[22,25]
Robotics	Monitoring linear robot stability and motion accuracy	Adaptability to various robotic configurations, high precision	[17]
Seismic Monitoring	Displacement and stress measurement under seismic excitation	Highly sensitive, suitable for dynamic environments	[19,33]

3. Working Principle of Fiber Bragg Gratings

FBGs are created by exposing the core of a single-mode optical fiber to a regular pattern of intense ultraviolet (UV) laser light. Ultraviolet light permanently alters the fiber core's refractive index, resulting in periodic modulation. This modulation occurs at the micrometer scale, resulting in an alternating pattern of regions with higher and lower refractive indices within the fiber. The periodicity of variations in the refractive index, known as the grating period, is an important aspect influencing the grating's responsiveness to external stimuli.

As light travels through the fiber, a small amount is reflected at each periodic modulation point. The spacing of the grating periods and the refractive index of the fiber determine the wavelength of reflected light. When the grating period meets the Bragg criterion, the constructive interference of reflected light is at its maximum. This condition is differentiated by equation (1).

$$\lambda_{Bragg} = 2n\delta \tag{1}$$

In this case, λ_{Bragg} signifies the Bragg wavelength; n relates to the effective refractive index of the fiber core; and δ represents the grating period. Under the Bragg condition, light at the Bragg wavelength is heavily reflected, whereas light at other wavelengths passes through the grating with little loss. Environmental factors such as temperature and strain have a significant impact on the wavelength of reflection, altering the effective refractive index (n) and the grating period δ. Fig. 1 depicts the principle of light reflection and transmission within the fiber.

Upon interaction with the grating, only those wavelengths that satisfy the Bragg condition are reflected back to the source. The reflected wavelengths experience minimal attenuation and directly indicate changes in the fiber's environment. FBGs are highly effective for sensing applications, as even slight variations in temperature or strain result in noticeable alterations in the reflected wavelength.

The key advantage of FBGs is their ability to provide highly precise and localized strain and temperature data. The sensitivity of the Bragg wavelength is due to variations in the fiber's refractive index, which are impacted by strain and temperature, as well as changes in the grating period caused by the fiber material's thermal expansion.

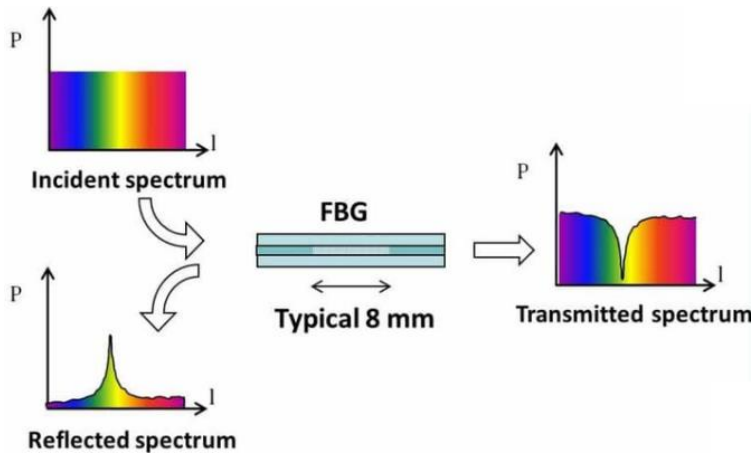

Fig. 1 Working principle of FBG

FBG sensors demonstrate a shift in the Bragg wavelength as a result of variations in temperature and mechanical strain. The coupled effects can be characterized by the stress-optic effect and the thermo-optic effect. The stress-optic effect occurs when mechanical strain is applied to the fiber, resulting in changes in both the grating period and the effective refractive index. The alteration in the grating period and the variation in

refractive index result in a shift of the Bragg wavelength. Temperature variations influence the refractive index of the fiber through the thermo-optic effect, while the thermal expansion of the fiber material affects the grating period. The effects of temperature and strain can be quantitatively represented by equation (2).

$$\frac{\Delta\lambda(\in,T)}{\lambda_B} = (1-p_e)\cdot\in+(\alpha+\xi)\cdot\delta T \tag{2}$$

Where $\Delta\lambda(\in, T)$ represents the variation in Bragg wavelength resulting from strain $\in$ and temperature T. The original Bragg wavelength is denoted as λ_B, while p_e refers to the photo-elastic coefficient. Furthermore, α indicates the thermal expansion coefficient, and ξ indicates the thermo-optical coefficient. The parameters are essential to comprehend the influence of external factors on the performance of FBG sensors. Fig. 2 illustrates the correlation between Bragg wavelength shift and strain, emphasizing the direct proportionality between the applied strain and the resulting wavelength shift.

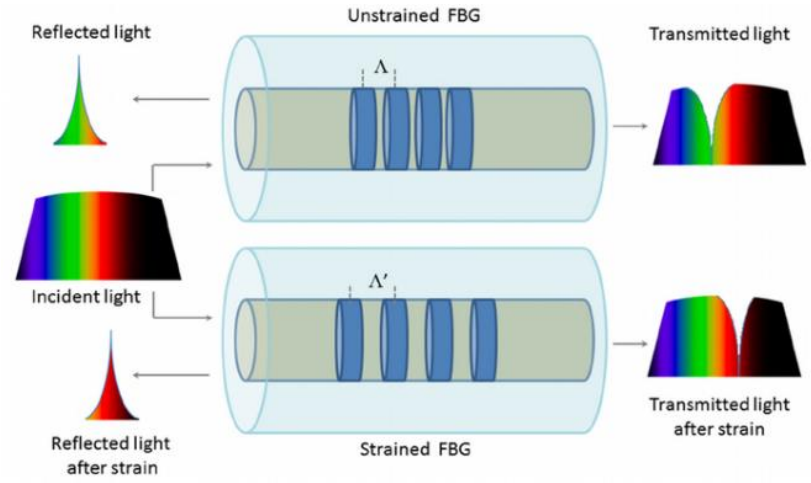

Fig. 2 FBG response as function of strain

A notable challenge in employing FBGs for sensing applications is the difficulty in differentiating the impacts of temperature and strain, as both affect the Bragg wavelength in analogous manners. The issue is the result of temperature fluctuations that induce modifications in both the refractive index and the grating period, which are comparable to the consequences of mechanical stress.

In response to this challenge, a range of compensation techniques have been developed. One method involves employing dual FBG sensors: one calibrated for temperature sensitivity and the other for mechanical strain detection. The strain-induced shift can be isolated by subtracting the temperature-sensitive FBG response from the total response. In situations where temperature and strain must be measured simultaneously, FBGs can be used in conjunction with other sensor technologies or advanced signal processing techniques to separate the effects.

4. FBG BASED VIBRATION MONITORING ARCHITECTURE

This section describes a vibration monitoring architecture utilizing a fiber Bragg grating (FBG), as illustrated in Fig. 3. This architecture is crucial for protecting buildings against damage and for initiating responses when vibrations exceed a specified threshold. The architecture primarily comprises the following modules:

- FBG sensor arrays: Each FBG sensor array is connected to an optical fiber. Depending on the monitored structure and application type, a single or multiple FBG arrays may be utilized. An FBG array comprises identical FBG sensors uniformly spaced at a distance L. The number of FBG sensors used in each array varies according to the monitored region's dimensions and layout. Each FBG returns sections of the incident pulses to circulator port 2 at various times. The suggested FBG deployment approach makes use of wavelength division multiplexing (WDM) technology to organize the FBGs in a series format. Each FBG sensor receives its own section of the optical spectrum from the WDM network. As a result of the limited overall available spectrum, the spectral range assigned to each FBG sensor must be lowered in response to the increased number of sensors.
- Field Programmable Gate Array (FPGA): A physical unit that produces continuous optical pulses and selects the suitable FBG array for interrogation, as well as the pulse-generating frequency according to the application. The pulse generator module facilitates the generation of optical pulses across a range of wavelengths. Each wavelength denotes the central fiber Bragg grating wavelength.
- FBG interrogation module: The system comprises a circulator, an optical amplifier, and a light source. The optical pulse generator calibrates the laser source to produce n synchronized pulses, each of which corresponds to a specific wavelength. n is the number of FBG sensors in each array. The maximum vibration V_{max}, maximum amplitude A_{max}, and time slot allocation are regulated by an FPGA module. With a wavelength of n, a semiconductor optical amplifier (SOA) enhances a sequence of optical pulses. The pulse train is introduced into the FBG array by an optical circulator (C1). The time calculator module determines the duration of time required for optical pulses to be transmitted to the FBG array. Reduced time is required for the FBG interrogation module to acquire the reflected optical pulses.
- Data acquisition module: The reflected optical signals from the FBG sensors are collected by the data acquisition module. This enables the identification of the FBG associated with each incoming optical pulse. Fiber identifier, transmission timestamp, and receipt timestamp are the three components into which the data collection module categorizes the acquired signals. The pulse delay should not exceed the duration of the succeeding pulse. This necessitates the identification of the appropriate n reflection wavelengths for each fiber Bragg grating sensor in the array.
- Analysis module: For each FBG sensor, the analysis module computes the average horizontal and vertical vibrations V. It is imperative to track the evolution of the amplitude A (displacement) and the mean vibration values V of each FBG sensor over time. The prediction module initiates an alarm when these readings exceed predetermined thresholds.
- Prediction module: The prediction module's primary function is to predict critical events and locations by utilizing the estimated average vibration V. In order to prevent substantial structural harm, a warning is issued when V surpasses a chosen

threshold. Derived from the context of the application and the computed parameters, this module may possess specific sophisticated functionalities. The forecast module is capable of calculating the daily average vibration at the mid-span of a bridge during the sunnier months. The prediction module resembles a storage query system.

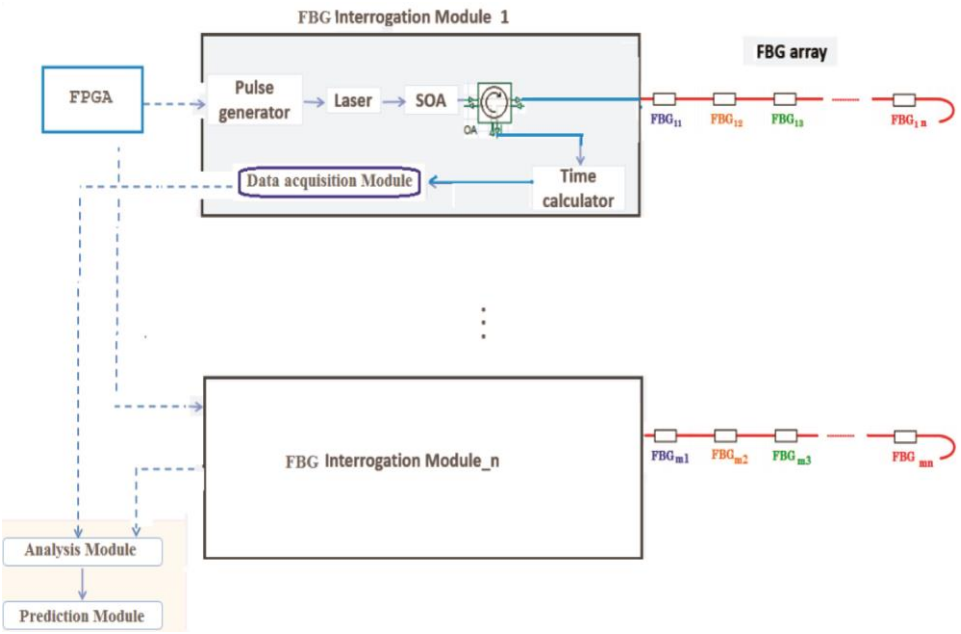

Fig. 3 FBG vibration monitoring architecture

5. Mathematics for FBG-Based Vibration Estimation

External factors, such as strain or temperature, can induce elongation or stretching in optical fibers. An FBG sensor detects external forces by measuring variations in the reflected wavelength spectrum. Consequently, accurate measurement of these displacements is essential for quantifying strain levels through the data collection module. Upon deformation, the signal reflected by the FBG returns with a wavelength of $\lambda_B + \delta\lambda$, where λ_B denotes the central FBG wavelength and $\delta\lambda$ signifies the wavelength shift. The reflected signal remains stable during the return, as the FBG sensors along the path do not impede it.

This study introduces a method to estimate the fiber deformation at a specific point in the FBG in response to external stress. An external strain applied to an optical fiber induces a proportional adjustment in the reflected wavelength of an FBG sensor. The strain influences the effective refractive index of a fiber Bragg grating (FBG), denoted as n, and the grating period, Λ, resulting in a variation of the reflected wavelength. Equation (3) demonstrates the relationship between the strain and the resulting wavelength shift.

$$\frac{\Delta\lambda}{\lambda_B} = (1 - p_e) \cdot \in \tag{3}$$

where $\Delta\lambda$ is the wavelength shift, λ_B is the FBG central wavelength, p_e is the strain-optic coefficient, and ϵ is the strain experienced by the FBG sensor.

In order to estimate the fiber deformation under strain, we consider in our monitoring architecture two types of FBG nodes:

- FBG sensor nodes are strategically positioned in important locations inside the monitored structure. We specifically want to calculate the displacement and average vibration at these FBG nodes.
- FBG nodes that facilitate vibration calculations. These nodes are located between two FBG sensor nodes to enhance the approximation of fiber deformation, as illustrated in Fig. 4. The distance d between two successive FBG support nodes is a critical parameter; a smaller d improves the accuracy of the fiber deformation approximation.

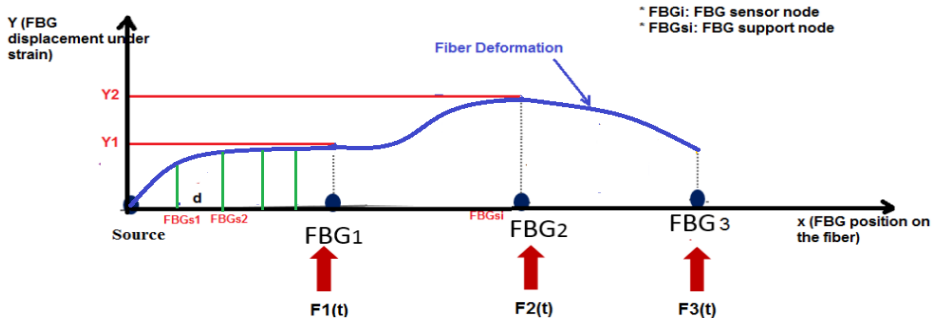

Fig. 4 Fiber deformation due to external forces

The fiber deformation can be represented by a curve when the distance L_i from the source to a sensor node FBG_i is substantial, as demonstrated in Fig. 5. To approximate the fiber with a segment, we suggest the discretization of the fiber using FBG support nodes. Therefore, the strain at each FBG sensor node FBG_i can be determined as follows [34]:

$$\epsilon_i = \frac{E_i}{L_i} \tag{4}$$

where L_i represents the initial length of the optical fiber from the source to the FBG_i sensor/support node, while E_i represents the deformation of the optical fiber extending from the source to the FBG_i sensor node.

As recorded by the FBG sensor node FBG_i, the strain exerted on the fiber at a specific site is indicated by the change in reflected wavelength. Upon receiving the reflected wavelength, the data acquisition module identifies the corresponding FBG node (sensor or support) and calculates the strain value for each FBG node based on the wavelength shift. The fiber's deformation from the source to each FBG sensor or support node is subsequently assessed. A method is introduced to estimate the displacement of the FBG sensor. The application of an external force perpendicular to the fiber is illustrated in Fig. 5. The subsequent equations define the displacement $y_i(t)$ of the FBG sensor/support node FBG_i, which is dependent on the value of the external force acting on the optical fiber. Based on the assumption that the fiber segment between two adjacent FBG sensors

or supports can be regarded as a linear segment, this is applicable when the FBGs are closely spaced and the monitored structure exhibits sufficient rigidity.

The accuracy of the fiber deformation approximation is improved by a decrease in the distance d between two consecutive FBG support nodes.

$$y_1(t) = \sqrt{E_1^2 - L^2} \tag{5}$$

If the intensity of the applied force increases in the FBG_i position compared to the FBG_{i-1} position, then $y_i(t)$ is given by:

$$y_i(t) = y_{i-1}(t) + \sqrt{(E_{i+1} - E_i)^2 - L^2} \tag{6}$$

If the intensity of the applied force decreases in the FBG_i position compared to the FBG_{i-1} position, then $y_i(t)$ is given by:

$$y_i(t) = y_{i-1}(t) - \sqrt{(E_{i+1} - E_i)^2 - L^2} \tag{7}$$

As a result, each FBG sensor node generates a set of displacements. Each observation moment, or time interval t, results in a displacement calculation. An observation shows the displacement of an FBG sensor along the y-axis at time t. This allows for the estimation of a displacement signal y_i for each FBG sensor. Fig. 5 illustrates how the displacements obtained can be extrapolated to derive the period and frequency of the displacement signal.

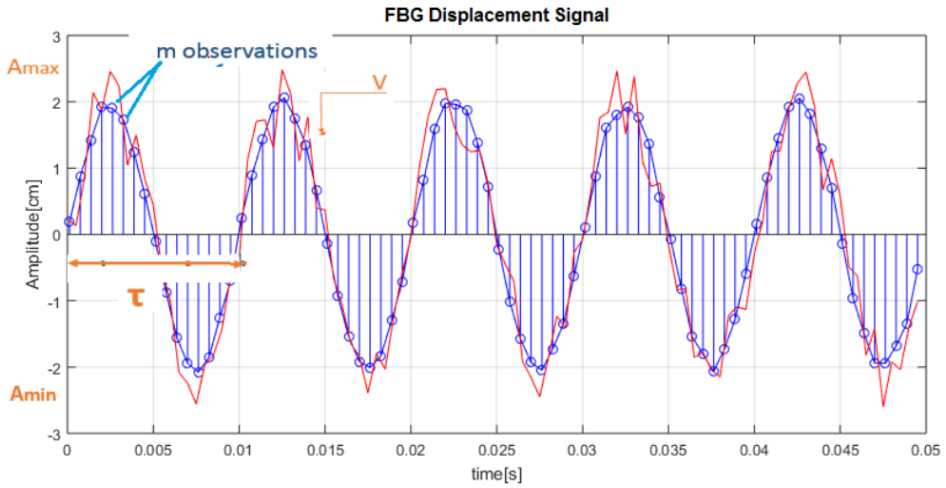

Fig. 5 Observation scheme

To determine the displacement signal $y_i(t)$ of FBG_i under the influence of an external force, such as vibration, it is essential to consider a specific time interval. The length of the slot is a critical variable in our vibration estimation methodology. The observed number of displacement points increases with a decrease in slot length. The maximum vibration amplitude is recorded with greater precision as the slot length diminishes.

If the phenomenon has a vibration character, with V is the frequency of the displacement signal of an FBG sensor and based on the following hypothesis:

- The vibration V is as follows: $V < V_{max}$ where V_{max} is the maximum vibration.
- The amplitude of the displacement signal A is as follows: $A < A_{max}$ where A_{max} is the maximum amplitude that causes damage to the structure.
- The pulse generation module generates a set of optical pulses in each time interval, which verifies: $slot > 1 / (m \cdot V_{max})$ with m the number of visible displacements.

Subsequently, we may calculate the mean vibration V_i for each FBG_i inside the fiber array, as well as the peak-to-peak amplitude P over a specified duration. The peak-to-peak amplitude P is defined as: $P = max_A - min_A$.

The observation time frame quantifies the vibration V_i of the FBG sensor FBG_i, as illustrated in Fig. 6. The number of observable displacements increases as the time interval s decreases. The estimated displacement signal FBG_i denoted as $y_i(t)$ enables measurement of the signal period τ_m. The increase in the number of observations approaches the true period τ_r, which reflects the actual vibration.

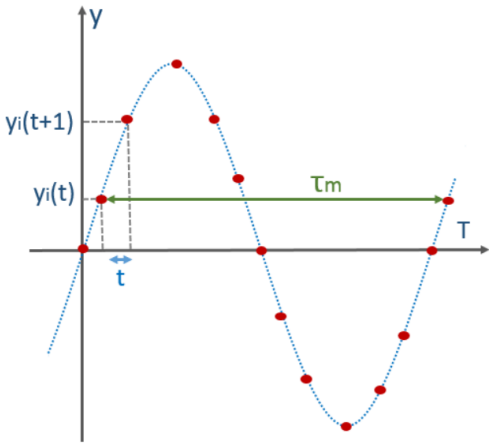

Fig. 6 Vibration estimation

The vibration is a continuous function within the time interval $[b, a_1]$. Let y_0 be a real number that lies between $Y(b)$ and $Y(a_1)$. If $Y(a_1) < 0$, then there exists at least one c such that $b \leq c \leq a_1$ and $y_0 = Y(c)$. Fig. 7 illustrates the application of intermediate value theory to estimate the period τ_m: $b_1 - b < \tau < a_1 - a$. Sinusoids cannot occur between two FBG displacements y_i due to the constraint that the maximum vibration is limited to V_{max}, which is associated with the minimum period τ_{min} ($\tau_{min} = 1/V_{max}$). Therefore, the intermediate value theorem can be employed to approximate the period τ_m.

To estimate the amplitude at a specific instant t, we note that c_r denotes the maximum amplitude (Fig. 7), which may be uncertain due to possible measurement inaccuracies at that moment; nonetheless, it is greater than the recorded values c_1 and c_2. However, c_r is less than both $c_1 + \Delta A_{max}$ and $c_2 + \Delta A_{max}$, where ΔA_{max} denotes the maximum increase in amplitude over the duration of the pulse m / τ_m, leading to the subsequent inequality: $c_1, c_2 \leq c_r \leq max\ (c_1, c_2) + \Delta A_{max}$.

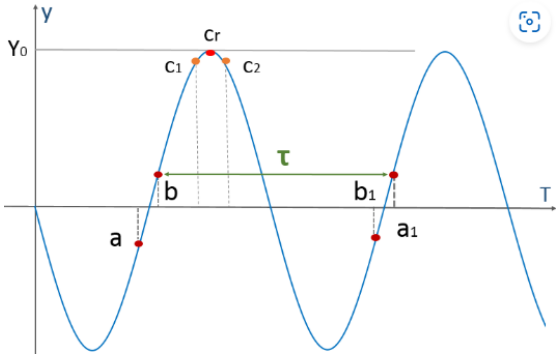

Fig. 7 Amplitude and periode estimation

6. Towards a Real Vibration Estimation System

6.1. System conception methodology

The proposed method overcomes obstacles in vibration monitoring by allowing for the estimation of average vibrations at critical locations within the fiber. The following steps comprise a vibration monitoring methodology that we suggest:

1. Implementing the physical network architecture begins with determining the location and number of FBG sensor nodes within the monitored structure. Second, we must determine how many optical fiber arrays will be constructed, as well as the number of FBG sensor nodes per array.
2. System configuration: This step consists on the optical system parameters' configuration which are mainly:
   - The number of generated pulses per second m by the optical source.
   - The maximum vibration value V_{max} that causes damage to the structure.
   - The maximum value of the amplitude A_{max} that causes damage to the structure.
   - ΔA_{max} is the maximum increase in amplitude during the duration of the pulse m / τ_m, where τ_m is the period of the displacement signal $y_i(t)$.
3. Average vibration estimation: The proposed approach comprises estimating the elongation L_i in each optical fiber segment (between two FBG sensors) to calculate the displacement signal $y_i(t)$ for each FBG_i over a given observation time. Using the predicted displacement signal $y_i(t)$ and the equations provided in the preceding sections, we compute the peak-to-peak displacement p_i and average vibration V_i over a given time period.

The parameters outlined are crucial for the construction of a vibration monitoring system; however, other features may be incorporated depending on the particular application and the objectives of the monitoring system. A vibration monitoring system has several goals, leading to distinct dimensional characteristics customized to each individual goal. Every vibration detection application requires a distinct deployment model for the FBG sensor network. Bridge vibrations typically result from the effects of traffic, wind, earthquakes, and their interactions.

6.2. Case study

This section analyzes the case study of the Vincent Thomas Bridge (VTB), a suspension bridge across the main channel of Los Angeles Harbor in San Pedro, California. The bridge illustrated in Fig. 8 was constructed in the early 1960s, measuring roughly 1850 m in total length and comprising three spans. The main span is 457.2 meters, while the surrounding spans on both sides are each 154 meters long. The bridge provides access to Terminal Island in the Port of Los Angeles and is a major traffic nightmare. The foundation consists of two steel pylons, each approximately 102.5 meters in height, two cable bends located at the eastern and western ends of the bridge, and concrete anchors for the main suspension cable. The pylons are erected on top of steel piles.

Fig. 8 Vincent Thomas Bridge (VTB)

Recent earthquakes have inflicted structural and foundational damage on bridges, resulting in considerable repair costs and prolonged traffic interruptions, hence causing large indirect losses in the impacted area. We employ the system conception method described in the previous section to monitor the vibrations of the VTB bridge induced by earthquakes, as seen in Fig. 9:

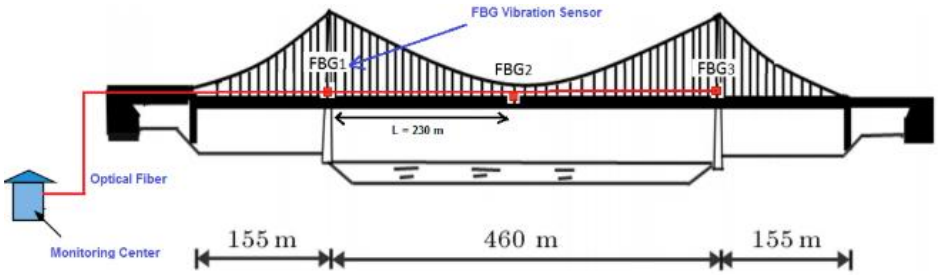

Fig. 9 Vibration monitoring system deployement on the VTB bridge

- The physical network comprises three FBG sensor nodes strategically positioned on the bridge suspension cables to facilitate vibration monitoring. The three FBG nodes are placed on an optical fiber array and are separated by a distance of L = 230 m.

- System configuration: At this stage, we need to configure the subsequent parameters: The minimum duration is 0.3 seconds, the pulse frequency m is set at 6 per second, the maximum vibration value V_{max} is determined as 1 / 0.3, and the maximum amplitude A_{max} is 15 cm.
- Average vibration estimation: Using existing equations, we can determine the peak-to-peak displacement P_i, the maximum amplitude A_i, and the average vibration V_i for a FBG_i sensor within a specified observation time window.

7. System Validation

7.1. Parameter's validation

This section assesses the performance of the proposed FBG design based on several parameters: the number of wavelengths per fiber, the inter-FBG distance d, the elasticity of the optical fiber and the maximum fiber length.

- The proposed deployment method for FBGs employs wavelength division multiplexing (WDM) to facilitate series connection of the installed FBGs. Each FBG sensor within the WDM network is allocated a distinct segment of the optical spectrum. With an increase in the number of sensors, the spectral bandwidth assigned to each individual FBG must be reduced because of the constraints of the total available source spectrum. The FBG interrogation module transmits laser pulses of different wavelengths to each FBG sensor node. Dense Wavelength Division Multiplexing (DWDM) facilitates the utilization of up to 320 wavelength channels.
- The variable d denotes the distance between two FBGs support nodes. The minimum distance between the inter-FBG support nodes, d, must be equal to l_0. In fact, the inequality $d / c > t_0$ holds, where c denotes the speed of light and t_0 means the minimum time interval, defined as $\tau_{min} = 1 / V_{max}$, with V_{max} representing the maximum allowed vibration. Consequently, l_0 is defined as c / V_{max} to avoid the overlap of reflected signals within the same time frame.
- Elasticity of optical fibers: The vibration sensing design incorporates elastic optical fibers that are capable of enduring significant elastic deformations, which are increasingly relevant in various applications.
- Maximum fiber length: The attenuation and dispersion of a fiber cable restrict the transmission distance without the use of an amplifier or repeater. The implementation of fiber amplifiers and dispersion compensators enhances the fiber length.

7.2. Design of the optical monitoring circuit

This section assesses the vibration detection capabilities of the FBG-based vibration monitoring network. The design has been completed using the OptiSystem tool, as illustrated in Fig. 10. This study examines a bit rate of 1000 bits per second utilizing a non-return-to-zero (NRZ) pulse generator. A Mach-Zehnder modulator was employed to modulate the continuous light produced by a continuous-wave laser operating at a frequency of 193.1 THz, with an intensity of 20 dBm. Subsequent to amplification by the Erbium-Doped Fiber Amplifier (EDFA), the light wave is directed into an optical circulator.

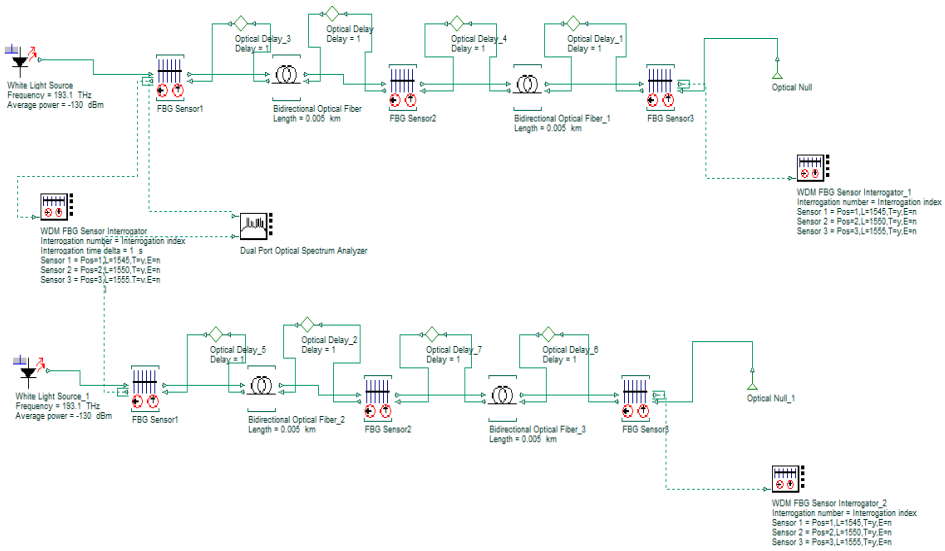

Fig. 10 Prototype of the vibration monitoring system

A 10 m single-mode fiber interlinks three identical fiber Bragg gratings, constituting a fiber Bragg grating sensing array. The separation between two adjacent FBGs in the array is 5 meters. The impact of vibration can be assessed by strain measurement. This study examines the impact of various strains on the wavelength shift in different FBG sensors. Fig. 11 illustrates the effect of wavelength alteration.

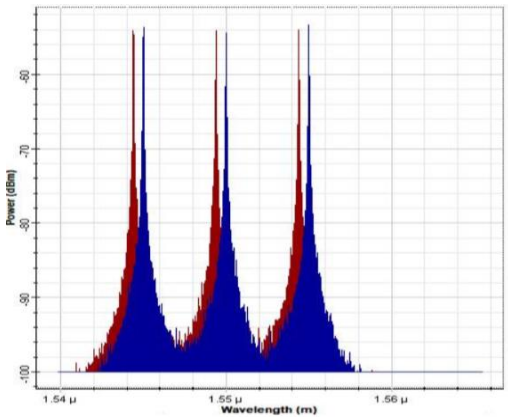

Fig. 11 Reflected spectrum shift under applied strain

8. Simulation Results

This section assesses the effectiveness of the proposed FBG-based vibration monitoring system. This study analyzes the Vincent-Thomas Bridge and the deployment model that clarifies the effects of the earthquake on the structure (Fig. 9). The simulation parameters are detailed below.

- The number of FBGs deployed is 3.
- The distance between FBG L is equal to 230 m. The distance L is derived from actual field measurements and structural analysis of the monitored infrastructure. This distance was chosen to ensure optimal sensitivity and coverage while minimizing redundancy in vibration detection.
- One FBG sensor array is considered.
- The minimal period is equal to 0.3 seconds.
- The maximum vibration value V_{max} is set to 1/0.3.
- The maximum amplitude value A_{max} is fixed to 15 cm.

In addition, empirical data from the Vincent-Thomas bridge was used in the analysis after the 2010 Calexico earthquake. The Center for Engineering Strong Motion Data provides access to these signals. Fig. 12 illustrates the obtained displacement signals from the localized sensor nodes over time, as specified in the deployment model (Fig. 9). The highest measured vibration amplitude is 11.102 cm in FBG2, located at the bridge's mid-span. The vibration amplitude is reduced at FBG1 (3.956 cm) and FBG3 (4.052 cm), located at the extremities of the bridge.

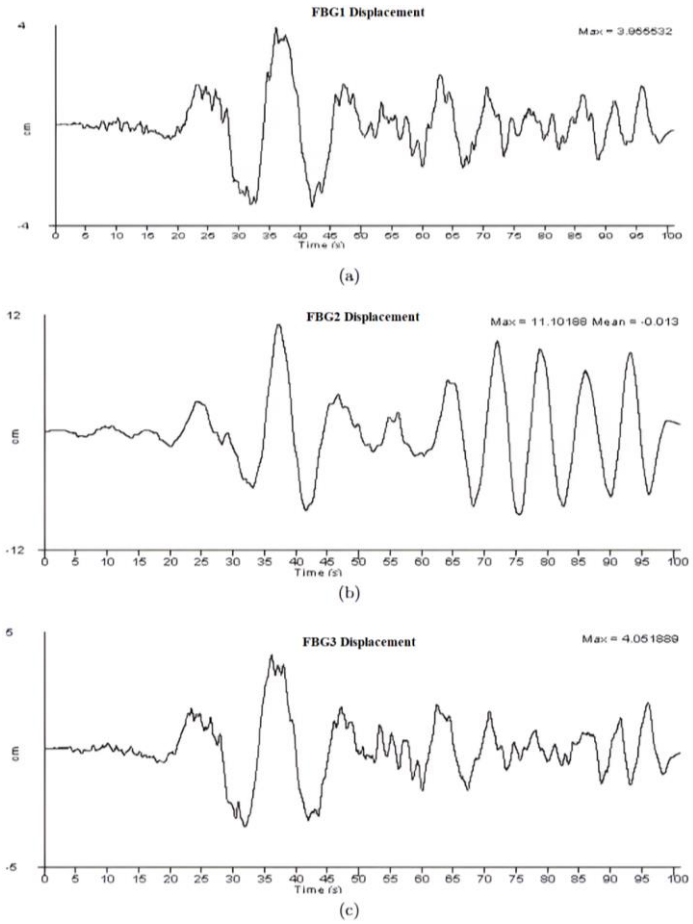

Fig. 12 FBG sensor displacements

Fig. 13 depicts the peak-to-peak displacement computed for the three FBG sensor nodes. The peak-to-peak displacement refers to the difference between the maximum and minimum displacements of an FBG sensor y within a specified time frame. The results indicate that the maximum peak-to-peak displacement is observed in the mid-span FBG (FBG_2). The earthquake has a greater effect on FBG_2 compared to the other FBG nodes situated at the two ends of the bridge.

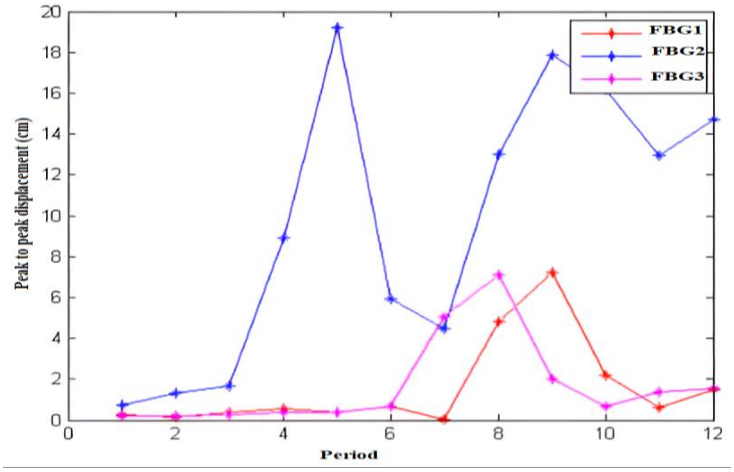

Fig. 13 Peak to peak displacement

Fig. 14 and 15 represent the calculated FBG1 displacements for the observation numbers $m = 4$ and $m = 6$, respectively. The anticipated displacement amplitude y_n for $m = 6$ exceeds that for $m = 4$. The error in the amplitude estimates decreases as the number of observations m for each instance increases.

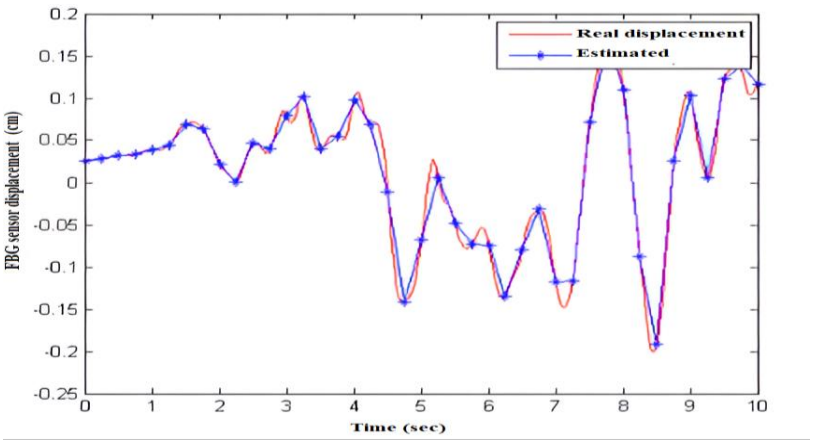

Fig. 14 FBG1 displacement's extrapolation with $m = 4$

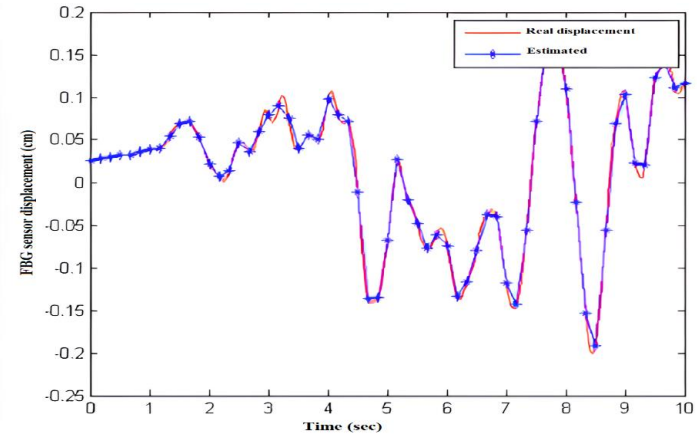

Fig. 15 FBG1 displacement's extrapolation with $m = 6$

Fig. 16 shows the amplitude error in relation to the number of observations m for each period τ_{min}. The approximation involves calculating the area between the two curves that represent the original vibration signal and the interpolated signal derived from the FBG displacements. The MATLAB function trapz(X, Y) employs trapezoidal integration to calculate the integral of Y with respect to X. The amplitude error decreases markedly as the number of observations m increases. As m grows, the measurements of the displacements of the FBG become increasingly precise, accurately representing the true state of vibration.

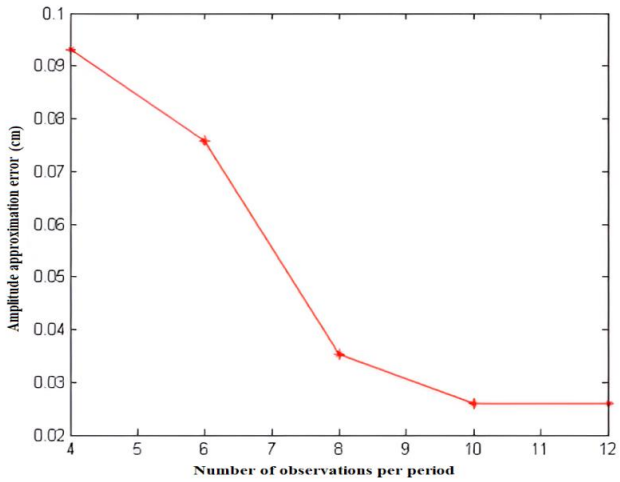

Fig. 16 Amplitude approximation error

Fig. 17 illustrates the deformation of an optical fiber induced by external forces, encompassing strain. This study examines three FBG support nodes positioned between two FBG sensors, FBG_1 and FBG_2, at intervals of 2.75, 5.5, and 8.25 meters, respectively.

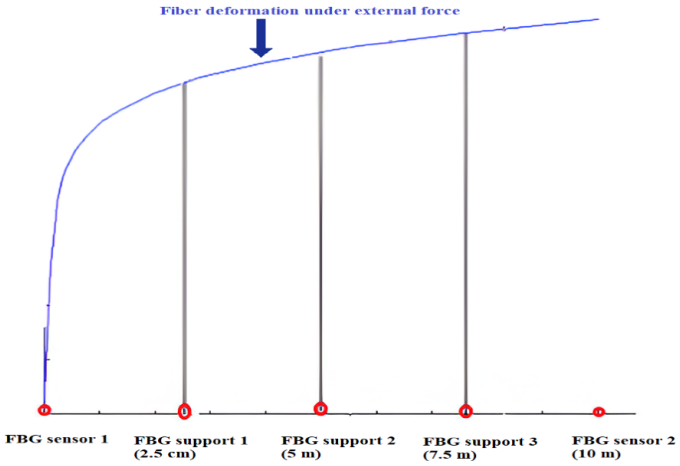

Fig. 17 Optical fiber deformation

Fig. 18 illustrates the relationship between the displacement estimation error at the FBG sensor node FBG_2 and the number of FBG support nodes. The displacement estimation error decreases with increasing number of FBG support nodes. Consequently, reducing the distance d between neighboring FBG support nodes produces a more precise representation of the FBG displacement, as the fiber segment between these nodes aligns linearly. Consequently, increasing the number of FBG support nodes improves the precision of displacement measurements at each FBG sensor. The allocation of wavelengths to each FBG node restricts the number of supporting FBG nodes.

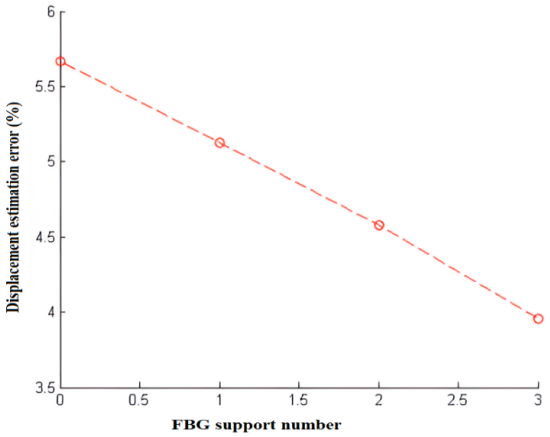

Fig 18. Displacement estimation error in terms of FBG support nodes number

9. CONCLUSION

This research introduces a universal method for vibration monitoring. This technique outlines the process for constructing the physical network architecture, designing the system design, and evaluating the vibration levels. The suggested methodology for vibration monitoring is applicable to many applications and architectural designs. The aforementioned example was derived from an actual research case related to the Vincent-Thomas Bridge (VTB).

This study examines a vibration monitoring system that uses Bragg fiber gratings for real-time vibration evaluation. This design improves the structural integrity of the structures. This design provides a method for estimating the fiber deformation, the FBG displacement, and the average FBG vibration. This methodology is based on the proposed framework. An approach for detecting vibrations has been proposed, employing the physical characteristics of FBG, which are significantly influenced by external strain.

As a future work, we can develop the prediction module. Thus, upon reaching the threshold for vibration or displacement, this module generates notifications to mitigate structural vibration levels. We can also classify the normal and abnormal vibrations of the monitored structure using machine learning algorithms.

REFERENCES

[1] K. Ágoston, " Vibration Detection of the Electrical Motors Using Strain Gauges", *Procedia Technol.*, vol. 22, pp. 767-772, 2016.

[2] A. Sabato, M. Q. Feng, Y. Fukuda, D. L. Carní and G. Fortino, " A Novel Wireless Accelerometer Board for Measuring Low-Frequency and Low-Amplitude Structural Vibration", *IEEE Sensors J.*, vol. 16, pp. 2942–2949, May 2016.

[3] M. Biglar, M. Gromada, F. Stachowicz, and T. Trzepieciński, " Optimal Configuration of Piezoelectric Sensors and Actuators for Active Vibration Control of a Plate Using a Genetic Algorithm", *Acta Mechanica*, vol. 226, pp. 3451-34620, 2015.

[4] Z. Zhou, S. Xue, C. Wan and B. Wu, " Optimal Sensor Placement and Bi-Type Response Reconstruction for Structural Health Monitoring Using Long-Gauge FBG Strain Sensing Network ", *Structures*, vol. 63, p. 106406, 2024.

[5] T. Wu, G. Liu, S. Fu and F. Xing, " Recent Progress of Fiber-Optic Sensors for the Structural Health Monitoring of Civil Infrastructure", *Sensors*, vol. 20, no. 16, p. 4517, 2020.

[6] M. F. Bado and J. R. Casas, "A Review of Recent Distributed Optical Fiber Sensors Applications for Civil Engineering Structural Health Monitoring", *Sensors*, vol. 21, no. 5, p. 1818, 2021.

[7] M. Sliti and N. Boudriga, " Structural Health Monitoring of Road Infrastructures Based on FBG Sensor Network", In Proceedings of the 27th Asia Pacific Conference on Communications (APCC), 2022, pp. 36-41.

[8] M. Sliti and N. Boudriga, " Aircraft Wing Vibration Monitoring Based on FBG Sensor Network", In Proceedings of the 19th International Multi-Conference on Systems, Signals & Devices (SSD), 2022, pp. 280-285.

[9] M. Sliti and N. Boudriga, " Building Structural Health Monitoring: An Fbg-Based Estimation of External Vibrations", In Proceedings of the 18th International Multi-Conference on Systems, Signals Devices (SSD), 2021, pp. 1026-1031.

[10] M. Sliti and N. Boudriga, "Bridge Structural Health Monitoring Using an FBG-Based Architecture", In Proceedings of the IEEE 64th International Midwest Symposium on Circuits and Systems (MWSCAS), 2021, pp. 621-625.

[11] M. A. Ibrar Jahan, et al., " Deciphering the Sensory Landscape: A Comparative Analysis of Fiber Bragg Grating and Strain Gauge Systems in Structural Health Monitoring ", *J.Optics*, 2024.

[12] C. Karatas, et al., "Fibre Bragg Grating Sensor Applications for Structural Health Monitoring", *Aircr. Eng. Aerosp. Technol.*, vol. 92, no. 3, pp. 355-367, 2018.

[13] M. H. Yassin, M. H. Farhat, R. Soleimanpour, et al., " Fiber Bragg Grating (FBG)-Based Sensors: A Review of Technology and Recent Applications in Structural Health Monitoring (SHM) of Civil Engineering Structures", *Discov. Civ. Eng.*, vol. 1, p. 151, 2024.

[14] Y. Zhou, D. Liu, D. Li, Y. Zhao, M. Zhang and W. Zhang, " Review on Structural Health Monitoring in Metal Aviation Based on Fiber Bragg Grating Sensing Technology", In Proceedings of Prognostics and Health Management Conference (PHM-Besançon), 2020, pp. 97-102.

[15] J. Alvarez-Montoya, A. Carvajal-Castrillón and J. Sierra-Pérez, " In-Flight and Wireless Damage Detection in a Uav Composite Wing Using Fiber Optic Sensors and Strain Field Pattern Recognition", *Mech. Syst. Signal Process.*, vol. 136, p. 106526, 2020.

[16] H.-W. Ho, W.-H. Liao, C.-Y. Chang and C.-C. Ma, " Structural Health Monitoring of a Linear Robot by Fiber Bragg Grating Sensors and Cyber-Physical System", *Int. J. Adv. Manuf. Technol.*, vol. 122, pp. 3983-3995, 2022.

[17] X. Gao, C. Tao, Y. Zhu, J. Li, Y. Wu, P. Huang, C. Feng, H. Wang and W. Wang, " Fiber Bragg Grating Array-Based Shape Sensing for Structural Health Monitoring of Cylindrical Marine Structures", In Proceedings of the Smart Structures and Materials + Nondestructive Evaluation and Health Monitoring, 2022, p. 1204617.

[18] S. Saha, S. A. Hadigheh, I. Rukhlenko, M. Valix, B. Uy and S. Fleming, " Machine Learning Augmented Multi-Arrayed Fiber Bragg Grating Sensors for Enhanced Structural Health Monitoring by Discriminating Strain and Temperature Variations", *J. Civil Struct. Health Monit.*, vol. 15, pp. 597-618, 2024.

[19] Z. Lei, L. Zhu, Y. Fang, C. Niu and Y. Zhao, " Fiber Bragg Grating Smart Material and Structural Health Monitoring System Based on Digital Twin Drive", *J. Nanomater.*, vol. 2022, p. 4356974, 2022.

[20] M. A. I. Jahan, R. Honnungar, V. L. Nandhini, V. L. Malini, H. Vohra, V. R. Balaji and S. K. Royc, "Deciphering the Sensory Landscape: A Comparative Analysis of Fiber Bragg Grating and Strain Gauge Systems in Structural Health Monitoring ", *J. Optics*, 2024.

[21] Q. Wu, Y. Okabe and F. Yu, " Ultrasonic Structural Health Monitoring Using Fiber Bragg Grating", *Sensors*, vol. 18, no. 10, p. 3995, 2018.

[22] R. N. Soman and W. M. Ostachowicz, " Ultrasonic Fiber Bragg Grating Sensor Placement Optimization in Structural Health Monitoring Using Covariance Matrix Adaptation Evolutionary Strategy", In Proceedings of Smart Structures and Materials + Nondestructive Evaluation and Health Monitoring, 2021, p. 115931A.

[23] L. Wang, C. Xiao, W. Ding, J. Wu, and C. Shi, " Application Overview of Fiber Bragg Grating Sensors in Structural Health Monitoring", In Proceedings of the IEEE 6th Advanced Information Technology, Electronic and Automation Control Conference (IAEAC), 2022, pp. 1946-1950.

[24] J. Braunfelds, U. Senkans, P. Skels, R. Janeliukstis, J. Porins, S. Spolitis, and V. Bobrovs, " Road Pavement Structural Health Monitoring by Embedded Fiber-Bragg-Grating-Based Optical Sensors", *Sensors*, vol. 22, no. 12, p. 4581, 2022.

[25] W. Jinghong, Y. Shaomin, Z. Jiqing, Z. Qing and Z. Wenxuan, "Structural Health Monitoring of Large-Section Tunnel of Jingxiong High-Speed Railway Based on Fiber Bragg Grating Monitoring Technology", *Laser Optoelectron. Prog.*, vol. 57, no. 21, p. 210603, 2020.

[26] Y.-Y. Ko, W.-K. Chang, K.-Y. Liu, H.-H. Hung and K.-C. Chang, "Damage Evaluation for RC Bridge Piers Using Vibration Measurement", *Adv. Struct. Eng.*, vol. 18, no. 9, pp. 1501-1515, 2015.

[27] F. Xiao, D. Meng, Y. Yu, Y. Ding, L. Zhang, G. S. Chen, W. Zatar and J. L. Hulsey, "Estimation of Vehicle-Induced Bridge Dynamic Responses Using Fiber Bragg Grating Strain Gages", *Sci. Prog.*, vol. 103, no. 1, p. 0036850419874201, 2019.

[28] Q. Nan, S. Li, Y. Yao, Z. Li, H. Wang, L. Wang and L. Sun, "A Novel Monitoring Approach for Train Tracking and Incursion Detection in Underground Structures Based on Ultra-Weak Fbg Sensing Array", *Sensors*, vol. 19, no. 12, p. 2666, 2019.

[29] S. Goossens, B. D. Pauw, T. Geernaert, M. S. Salmanpour, Z. S. Khodaei, E. Karachalios, D. Saenz-Castillo, H. Thienpont and F. Berghmans, Aerospace-Grade Surface Mounted Optical Fibre Strain Sensor for Structural Health Monitoring on Composite Structures Evaluated Against In-Flight Conditions", *Smart Mater. Struct.*, vol. 28, p. 065008, May 2019.

[30] Z. Liu, P. Liu, C. Zhou, Y. Huang and L. Zhang, " Structural Health Monitoring of Underground Structures in Reclamation Area Using Fiber Bragg Grating Sensors ", *Sensors*, vol. 19, no. 13, p. 2849, 2019.

[31] L. Xin, Z. Li, X. Gui, X. Fu, M. Fan, J. Wang and H. Wang, "Surface Intrusion Event Identification for Subway Tunnels Using Ultra-Weak Fbg Array Based Fiber Sensing", *Opt. Express*, vol. 28, pp. 6794-6805, Mar. 2020.

[32] L. Pereira, I. Bourgeois, H. Rodrigues, H. Varum, and P. Antunes, " Fiber Bragg Grating Based Displacement Sensors With Low Visual Impact for Structural Health Monitoring Applications – Monastery of Batalha Case ", *Sens. Actuators A: Phys.*, vol. 368, p. 115117, 2024.

[33] A. Elkady, M. Seleemah and F. Ansari, "Structural Response of a Cable-Stayed Bridge Subjected to Lateral Seismic Excitations", *J. Civ. Struct. Health Monit.*, vol. 8, pp. 417-430, 2018.

[34] O. Frazão, S. Silva, A. Guerreiro, J. Santos, L. Ferreira and F. Araújo, "Strain Sensitivity Control of Fiber Bragg Grating Structures With Fused Tapers", *Appl. Optics*, vol. 46, pp. 8578-8582, 2008.